

# CARBON ABUNDANCES OF THREE CARBON-ENHANCED METAL-POOR STARS FROM HIGH-RESOLUTION GEMINI-S/bHROS SPECTRA OF THE $\lambda 8727$ [C I] LINE

Simon C. Schuler<sup>1,2</sup>, Steven J. Margheim<sup>3</sup>, Thirupathi Sivarani<sup>4</sup>, Martin Asplund<sup>5</sup>, Verne V. Smith<sup>1</sup>, Katia Cunha<sup>1,6</sup>, AND Timothy C. Beers<sup>4</sup>

## ABSTRACT

We present the results from an analysis of the  $\lambda 8727$  forbidden [C I] line in high-resolution Gemini-S/bHROS spectra of three Carbon-Enhanced Metal-Poor (CEMP) stars. Previous derivations of C abundances in CEMP stars primarily have used the blue bands of CH and the C<sub>2</sub> Swan system, features which are suspected to be sensitive to photospheric temperature inhomogeneities (the so-called 3D effects). We find the [C/Fe] ratios based on the [C I] abundances of the two most Fe-rich stars in our sample (HE 0507-1653: [Fe/H] =  $-1.42$  and HE 0054-2542: [Fe/H] =  $-2.66$ ) to be in good agreement with previously determined values. For the most Fe-deficient star in our sample (HE 1005-1439: [Fe/H] =  $-3.08$ ), however, the [C/Fe] ratio is found to be 0.34 dex lower than the published molecular-based value. We have carried out 3D local thermodynamic equilibrium (LTE) calculations for [C I], and the resulting corrections are found to be modest for all three stars, suggesting that the discrepancy between the [C I] and molecular-based C abundances of HE 1005-1439 is due to more severe 3D effects on the molecular lines. Carbon abundances are also derived from

---

<sup>1</sup>National Optical Astronomy Observatory/Cerro Tololo Inter-American Observatory. Casilla 603, La Serena, Chile: sschuler@ctio.noao.edu, vsmith@noao.edu, cunha@noao.edu

<sup>2</sup>Leo Goldberg Fellow

<sup>3</sup>Gemini Observatory, Casilla 603, La Serena, Chile: smargheim@gemini.edu

<sup>4</sup>Department of Physics and Astronomy, Center for the Study of Cosmic Evolution, and Joint Institute for Nuclear Astrophysics, Michigan State University, East Lansing, MI: thirupathi@pa.msu.edu, beers@pa.msu.edu

<sup>5</sup>Max Planck Institute for Astrophysics, Postfach 1317, 85741, Garching, Germany: asplund@mpa-garching.mpg.de

<sup>6</sup>On leave from Observatório Nacional, Rio de Janeiro, Brazil

C I high-excitation lines and are found to be 0.45 – 0.64 dex higher than the [C I]-based abundances. Previously published non-LTE (NLTE) C I abundance corrections bring the [C I] and C I abundances into better agreement; however, targeted NLTE calculations for CEMP stars are clearly needed. We have also derived the abundances of nitrogen, potassium, and iron for each star. The Fe abundances agree well with previously derived values, and the K abundances are similar to those of C-normal metal-poor stars. Nitrogen abundances have been derived from resolved lines of the CN red system assuming the C abundances derived from the [C I] feature. The abundances are found to be approximately 0.44 dex larger than literature values, which have been derived from CN blue bands near 3880 and 4215 Å. We discuss evidence that suggests that analyses of the CN blue system bands underestimate the N abundances of metal-poor giants.

*Subject headings:* stars:individual (HE 0054-2542, HE 0507-1653, HE 1005-1439)  
 — stars:abundances — stars:atmospheres — stars:carbon — stars:Population II

## 1. INTRODUCTION

The discovery that a significant fraction of very metal-poor (VMP;  $[\text{Fe}/\text{H}] \leq -2.0$ ) stars have highly enhanced abundances of carbon ( $[\text{C}/\text{Fe}] \geq +1.0$ ) has spurred vigorous research efforts focused on delineating the nucleosynthetic histories of these objects and their role in the chemical evolution of the Galaxy. The actual fraction of VMP stars that are carbon-enhanced has yet to be precisely determined, but current estimates range from  $\sim 10\%$  to  $\sim 25\%$  (Cohen et al. 2005; Marsteller et al. 2005; Frebel et al. 2006; Lucatello et al. 2006). This fraction rises at lower metallicities, reaching  $\sim 40\%$  of stars with  $[\text{Fe}/\text{H}] \leq -3.5$ , and stars with  $[\text{Fe}/\text{H}] < -4.0$ , only three of which are currently known, are all carbon-enhanced. The increasing incidence of carbon enhancement at lower and lower metallicities implies that the nucleosynthetic pathway(s) leading to these Carbon-Enhanced Metal-Poor (CEMP) stars is highly efficient at low metallicities and that it played an important role in the nucleosynthetic history of the early Galaxy. Indeed, the fraction of CEMP stars as a function of metallicity may have critical implications for the initial mass function (IMF) in the early Universe (Tumlinson 2007).

The manner in which the majority of VMP stars are discovered, and how CEMP stars are subsequently identified, follows a well established procedure<sup>6</sup>. Stars are first tagged as VMP candidates based on the strength of the Ca II K line in low-resolution spectra from objective-prism surveys, in particular the HK survey (Beers, Preston, & Shectman 1985, 1992; Beers 1999) and the Hamburg/ESO survey (HES; Wisotzki et al. 2000; Christlieb

2003). Medium-resolution spectra of the VMP candidates are then obtained and used to identify *bona fide* VMP stars within the sample. The medium-resolution spectrum of a given VMP star is used to estimate its metallicity ( $[\text{Fe}/\text{H}]$ ) by analyzing the strength of the Ca II K line as a function of the broadband colors of the star, and inspection of the CH G-band found at 4300 Å reveals whether or not the star is enhanced in C (e.g., Rossi et al. 2005). Estimates of a star’s C abundance can be obtained from the CH G-band; however, in the spectra of many CEMP stars, the G-band feature is sufficiently strong as to be saturated, rendering it incapable of providing accurate abundance determinations. In these cases, C<sub>2</sub> lines of the Swan system can be used instead to estimate C abundances. Once identified, VMP stars are often slated for high-resolution spectroscopic follow-up studies, with which more accurate abundances of Fe, C, and numerous other elements, as well as important ratios such as <sup>12</sup>C/<sup>13</sup>C, can be derived.

Analyses of C abundances in high-resolution spectroscopic follow-up studies of CEMP stars focus on the same molecular features as those analyzed in medium-resolution spectra, namely the blue bands of the CH and C<sub>2</sub> Swan systems, because it is the molecular features that stay strong and most easily measurable in the spectra of VMP giants. Another reason is that atomic C I lines result from high-excitation transitions, and if measurable, these lines are not believed to be accurate abundance indicators because of their sensitivity to non-local thermodynamic equilibrium (NLTE) effects (Asplund 2005; Fabbian et al. 2006). However, the abundances derived from the CH and C<sub>2</sub> features in the spectra of VMP stars using standard 1-dimensional (1D) local thermodynamic equilibrium (LTE) analyses may not be accurate either. Abundances derived from molecular features are generally very sensitive to the temperature structure of stellar atmosphere models, and studies of time-dependent 3-dimensional (3D) hydrodynamical models have shown that the molecular lines are susceptible to temperature inhomogeneities due to photospheric granulation, the so-called 3D effects (Asplund 2005). The effects on molecular lines are such that abundances based on 3D models are lower than those derived using 1D models, with differences as large as  $\sim 1.0$  dex at  $[\text{Fe}/\text{H}] = -3$  (Asplund & García Pérez 2001; Collet, Asplund, & Trampedach 2007).

The derivation of accurate C abundances of CEMP stars is essential to their proper characterization and subsequently to the correct interpretation of their role in the chemical evolution of the Galaxy. Here we present the results of our investigation into the accuracy of published C abundances as derived from CH and C<sub>2</sub> features by analyzing the forbidden [C I] line at 8727.13 Å in high-resolution Gemini-S/bHROS spectra of three CEMP stars:

---

<sup>6</sup>Here we describe the identification of metal-poor stars based on the low-resolution spectra of objective-prism surveys, the most prolific sources of VMP stars. For a description of other methods used to find metal-poor stars, please see Beers & Christlieb (2005).

HE 0054-2542 (CS 22942-019), HE 0507-1653, and HE 1005-1439. The  $\lambda 8727$  [C I] line is known to be immune to NLTE effects and to be a highly reliable abundance indicator (Gustafsson et al. 1999), and it has been used to derive the C abundance of the Sun (e.g., Lambert 1978; Allende Prieto, Lambert, & Asplund 2002; Asplund et al. 2005b), field dwarfs (e.g., Gustafsson et al. 1999; Bensby & Feltzing 2006), R Coronae Borealis stars (e.g., Pandey et al. 2004), and Cepheid variables (e.g., Luck & Lambert 1981). For CEMP stars, it provides an excellent benchmark for C abundances derived from molecular features.

## 2. ASTROPHYSICAL SPECTROSCOPY OF CARBON

Carbon abundances can be derived from both atomic and molecular features in the spectra of late-type stars. The available atomic lines include numerous high-excitation ( $\chi \geq 7.48$  eV) C I lines found throughout the optical and near-IR spectral regions and a single [C I] forbidden feature at  $8727.13 \text{ \AA}$ . Suitable molecular features include electronic and rotational-vibrational transitions of CH and  $C_2$ , which are also found throughout the optical and near-IR spectral regions. Deriving C abundances from CO and CN transitions is also possible, but prior knowledge of the stellar O and N abundances is needed. For CEMP stars, it is more often the case that the C abundance of a star is known from an analysis of CH or  $C_2$  features, and the CO and CN lines are used for the derivation of O and N abundances. However, for cool environments such as those found in the atmospheres of red giants, a significant fraction of C is tied up in CO, so C abundances derived from C I, [C I], CH and  $C_2$  lines can also be sensitive to the adopted O abundance. Below we discuss the two sets of atomic and molecular C features in the context of using them to derive accurate abundances, particularly of CEMP stars.

### 2.1. C I

The permitted neutral C lines in the spectra of late-type stars all originate from high-excitation transitions, and they all are sensitive to NLTE effects. The NLTE effects are such that C abundances are overestimated by LTE analyses (lines are weaker in LTE compared to NLTE), and thus NLTE corrections are negative. Detailed accounts of modeling the C atom and the nature of NLTE effects are given by Asplund (2005) and Fabbian et al. (2006).

The stellar parameter space for which NLTE effects and the high-excitation C I lines has been investigated is rather limited, but in general the published studies agree quite well. For solar-like stars (stars with similar  $T_{\text{eff}}$ ,  $\log g$ , and metallicity as the Sun), NLTE corrections

are typically -0.05 to -0.1 dex (Stürenburg & Holweger 1990; Asplund 2005; Takeda & Honda 2005; Fabbian et al. 2006). These corrections are predicted to increase in magnitude, i.e., become more negative, with increasing  $T_{\text{eff}}$  and decreasing  $\log g$ , as well as with increasing line strength. Metallicity apparently has a minor effect on predicted NLTE corrections, with the peak correction occurring near  $[\text{Fe}/\text{H}] = -1.0$  and then tapering off slightly by no more than 0.10 dex at  $[\text{Fe}/\text{H}] = -3.0$ . Interestingly, Fabbian et al. (2006) note that the assumed  $[\text{C}/\text{Fe}]$  ratio also affects the predicted NLTE corrections such that the magnitude of the corrections become larger for increasing  $[\text{C}/\text{Fe}]$  ratios since the line-formation region is shifted outwards in the atmospheres where the departures from LTE is more pronounced. One would thus expect this effect to be significant in the analysis of CEMP stars.

## 2.2. [C I]

The [C I] forbidden line results from a low-excitation ( $\chi = 1.26$  eV) electric quadrupole ( $D_2^1 - S_0^1$ ) transition in carbon’s ground state configuration ( $2s^2 2p^2$ ). The ground state of C I is populated according to Boltzmann statistics, and thus transitions from this state are formed in LTE. The next three energy levels, of which the [C I] transition arises from the first, are strongly coupled through collisions to the ground state, assuring that they too are in LTE (Stürenburg & Holweger 1990). For this reason, the [C I] line is expected to be a highly accurate abundance indicator and not susceptible to NLTE effects (e.g., Gustafsson et al. 1999).

Deriving accurate C abundances from the [C I] line is not without its challenges, however. Lambert & Swings (1967) preliminarily identified a possible blending Fe I line at 8727.10 Å, but along with subsequent authors (e.g. Gustafsson et al. 1999; Allende Prieto et al. 2002; Asplund et al. 2005b), they determined that the blending Fe I feature contributes negligibly to the [C I] line strength in the solar spectrum. However, for completeness, the blending feature should be included in the  $\lambda 8727$  linelist, particularly for stars with  $[\text{C}/\text{Fe}] < 0$ . Also, in the solar spectrum there is a strong ( $\sim 100$  mÅ) Si I line at 8728.01 Å, just 0.88 Å to the red of the [C I] feature. The Si I line can affect the continuum in the  $\lambda 8727$  region, making high-resolution spectroscopy essential to the accurate measurement of the [C I] line. Neither of these concerns is applicable to metal-poor stars, for which the blending Fe I and neighboring Si I features become increasingly weak at sub-solar metallicities. Unfortunately, the [C I] line also becomes weak at low metallicities, vanishingly so at  $[\text{Fe}/\text{H}] < -1.0$  (Akerman et al. 2004), *except* for CEMP stars. As we demonstrate below, the [C I] line can remain strong enough for reliable measurements in the spectra of CEMP stars down to at least  $[\text{Fe}/\text{H}] \sim -3.0$ .

As a final note, we point out that temperature inhomogeneities due to photospheric granulation, the so-called 3D effects, do not greatly affect abundances derived from neutral atomic C lines (Asplund 2005). The difference in the solar C abundance as derived from the [C I] line using 3D hydrodynamical LTE models and conventional 1D LTE models amounts to  $\lesssim 0.05$  dex (Asplund et al. 2005b). While the susceptibility of the [C I] line to LTE 3D effects as a function of metallicity has not been investigated, the high-excitation C I lines are expected to remain relatively impervious to them at all metallicities due to their large depths of formation (Asplund 2005).

### 2.3. CH and C<sub>2</sub>

These molecular features are likely relatively immune to NLTE effects, although little computational work has been done in this area (Asplund 2005). What is clear is that the molecular lines are highly sensitive to temperature inhomogeneities and by extension, 3D effects. For the Sun, 3D corrections for abundances derived from CH and C<sub>2</sub> lines have been estimated to range from 0.00 to -0.15 dex (1D abundances are higher), depending on the lines being analyzed (Asplund et al. 2005b). The divergence between C abundances derived from these molecular lines using 1D and 3D models grows with decreasing metallicity, reaching differences ranging from -0.5 to -0.8 dex for giants and sub-giants at [Fe/H] = -3 (Asplund 2005; Collet et al. 2007).

The susceptibility of the CH and C<sub>2</sub> features to 3D effects is unfortunate, because it is these lines that generally remain strong at low metallicities. Indeed, the CH band near 4300 Å and lines of the C<sub>2</sub> Swan system at 4730, 5170, and 5635 Å are the features most often used to derive C abundances of CEMP stars. Many authors have noted that the C abundances derived from these molecular features may be in error by as much as 0.60 dex or more (e.g., Aoki et al. 2007; Frebel et al. 2007), but because 3D hydrodynamical models tailored for CEMP stars have not been constructed, accurate corrections to 1D abundances cannot be made. This is the source of the motivation for the research presented in this paper. By deriving abundances from an accurate abundance indicator, the [C I] forbidden line, we can provide some insight into the relative accuracy of the C abundances derived from molecular lines in the spectra of CEMP stars.

### 3. OBSERVATIONS AND DATA REDUCTION

#### 3.1. Observations

Multiple spectra of three CEMP stars were taken on UT 2006 December 26 and 27 at the Gemini-S telescope with bHROS, the bench-mounted High-Resolution Optical Spectrograph. The spectrograph is located within a thermal enclosure in the pier lab of the Gemini-S telescope and is fiber-fed from the telescope’s Cassegrain focus via a fiber cassette inserted into the Gemini Multi-Object Spectrograph (GMOS-South). The object-only mode of operation was used for our observations; this mode utilizes a single  $0.9''$  fiber that feeds a dedicated image slicer to produce a ‘slit’ that is  $0.14''$  wide and  $\sim 6.5''$  long, projected to the camera focal plane. A slicer rotation mechanism is used to ensure a ‘vertical’ slit at the observed spectral wavelength. The spectrograph is cross-dispersed using a set of fused silica prisms to ensure the echelle orders are well separated on the detector, a single  $2048 \times 4608$  E2V CCD with  $13.5 \mu\text{m}$  pixels. The wavelength range over which bHROS is operational spans from 4000 to  $10,000 \text{ \AA}$ .

For our observations,  $4 \times 2$  (spatial direction  $\times$  dispersion direction) binning was used to reduce the spectrograph’s working resolution of  $R = \lambda/\delta\lambda = 150,000$  to an effective resolution of  $R = 75,000$  in order to increase the signal-to-noise (S/N) ratio of the spectra and to lessen the impact of read noise, which can be significant given the detector’s intrinsically high read noise of  $5.3 \text{ e}^-$  and wide spectral orders (200 unbinned pixels). The grating was configured to produce a central wavelength on the detector of  $8352 \text{ \AA}$ . In this configuration, incomplete coverage from  $7135 - 9170 \text{ \AA}$  was obtained over seven echelle orders. The continuous coverage available within a single order is about  $88 \text{ \AA}$ , depending on the order.

The spectra were obtained in queue operations during photometric conditions with optical seeing varying between  $0.35$  and  $0.8''$ , with the majority of the delivered image quality better than  $0.5''$ . The total exposure time was 9880s for HE 0054-2542 (3 exposures), 6280s for HE 0507-1653 (2 exposures), and 15900s for HE 1005-1439 (5 exposures); the S/N ratios of the combined spectra at  $8727 \text{ \AA}$  are 114 for HE 0054-2542, 149 for HE 0507-1653, and 65 for HE 1005-1439. A detailed observing log is presented in Table 1. In addition to our target spectra, we also obtained a calibration set of daily biases, flats, and ThAr arc spectra.

#### 3.2. Reductions

Processing of the spectra was completed following normal echelle reduction practices with standard IRAF packages, with careful adaptations to suit the bHROS data. The raw

spectra were bias corrected by overscan and bias image subtraction. The inter-order scattered light is typically  $\sim 5$  ADU and varies by only a few tenths of an ADU over 50 pixels, which is the width of our binned orders and much larger than the spectral features we are observing. Since the uncertainty in the smoothed fit to the scattered light is larger than the gradient in the scattered light, no scattered light correction was performed. Cosmic rays were removed using L.A. Cosmic (van Dokkum 2001). The images were then flat-fielded to remove both the pixel-to-pixel variations and fringing from our spectra. The E2V CCD used in bHROS suffers from severe fringing in the red. However, as the light path for the flat observations is identical to our target observations, the illumination pattern on the detector is constant, and the fringe pattern is consistent in all spectra. Thus, the fringe patterns in our spectra are very well removed in the flat fielding process.

The use of a prism cross-disperser combined with a long ‘slit length’ causes the spectral orders to be tilted severely away from the central order, potentially resulting in the loss of resolution during the extraction process. To reduce the impact of this tilt on the resolution of our extracted spectra, each of the seven spectral orders was divided into 14 sub-apertures (7 orders  $\times$  14 sub-apertures = 98 total sub-apertures), and then each sub-aperture was extracted individually using optimal extraction methods. The extracted spectra were then blaze corrected using the extracted flat field spectra. The individual orders of the ThAr spectra were also divided into 14 sub-apertures, and wavelength solutions were derived for each of the 98 sub-apertures. The typical RMS scatter of the dispersion solutions was 0.0025 pixels. The wavelength solutions and heliocentric velocity corrections were applied to the individual sub-apertures, which were then recombined into their respective orders, achieving a fully reduced 1-D echelle spectrum composed of seven spectral orders. Finally, the spectra were continuum normalized to produce our final spectra for analysis.

## 4. ANALYSIS

### 4.1. Stellar Parameters

Determining the physical parameters— $T_{\text{eff}}$  surface gravity ( $\log g$ ), and microturbulent velocity ( $\xi$ )—of a stellar sample is always a critical component of any chemical abundance analysis. In general, this is not a trivial exercise and requires spectra of sufficient quality and wavelength coverage to allow for the derivation of the parameters directly from the spectra themselves, and/or accurate photometry, color- $T_{\text{eff}}$  relations, and isochrones with which the parameters can be determined indirectly. For metal-poor stars, the spectroscopic method may not be an option at all due to the paucity of the necessary metal lines in their spectra. This is the case for our sample, and thus we have adopted stellar parameters appearing in

the recent literature. This has the added advantage of allowing a more direct comparison of our [C I]-based abundances to those derived previously. The adopted parameters for each star are given in Table 2 and are described here:

**HE 0054-2542:** This star, also known as CS 22942-019, has been studied by Preston & Sneden (2001) and Aoki et al. (2002c). Preston & Sneden used the Revised Yale Isochrones (Green et al. 1987) and the observed dereddened  $(B-V)_0$  colors, corrected for the blanketing effects of the strong molecular C bands in the B and V filter passbands, of their stellar sample to obtain initial values of  $T_{\text{eff}}$  and  $\log g$ . They then proceeded to refine the stellar parameters, including the microturbulent velocity, spectroscopically by requiring the abundances of Fe I, Fe II, and Ti II derived using high-resolution spectra of their sample to be independent on a line-by-line basis of line strength, excitation potential, and ionization state. This process was hampered by the modest S/N ratio and resolution of their spectra (typically  $S/N \sim 30$ ,  $R \sim 20,000$ ), and any adjustments to the initial parameter values were constrained to fall within the estimated parameter uncertainties. The final parameters adopted by them for HE 0054-2542 are  $T_{\text{eff}} = 4900$  K,  $\log g = 1.8$  (cgs),  $\xi = 2.0$  km s<sup>-1</sup>, and  $[\text{Fe}/\text{H}] = -2.67$ .

Aoki et al. (2002c) used broadband photometry and a temperature scale based on dereddened  $(B-V)_0$  colors devised for carbon-rich metal-poor stars by Aoki et al. (2002a) to estimate  $T_{\text{eff}}$  for their stellar sample. Surface gravities and microturbulent velocities were then derived spectroscopically using high-resolution spectra by forcing ionization balance between the abundances of Fe I and Fe II and demanding that line-by-line Fe I abundances were independent of equivalent width (EW). The resulting parameters found by Aoki et al. (2002c) for HE 0054-2542 are  $T_{\text{eff}} = 5000$  K,  $\log g = 2.4$  (cgs),  $\xi = 2.1$  km s<sup>-1</sup>, and  $[\text{Fe}/\text{H}] = -2.64$ .

The agreement in the stellar parameters between the Preston & Sneden (2001) and Aoki et al. (2002c) studies is quite good, with the possible exception of the surface gravity. Both groups derived  $\log g$  for this star spectroscopically, that is to say by forcing ionization balance; however, it is likely that the low signal-to-noise ratio and moderate resolution spectra of Preston & Sneden adversely affected their parameter derivations. Indeed, the authors point out that the line-to-line scatter in the individual abundances are typically 0.2 – 0.3 dex, which prevented them from doing a detailed assessment of their stellar parameters. Thus, we have adopted the  $\log g$  value for HE 0054-2542 derived by Aoki et al. (2002c), who used higher quality spectra in their analysis ( $R = 50,000$  and  $S/N \sim 60$ ). Likewise, we have adopted the  $T_{\text{eff}}$  and  $[\text{Fe}/\text{H}]$  abundance of Aoki et al. (2002c), along with  $\xi = 2.0$  km s<sup>-1</sup>, for this star.

**HE 0507-1653:** This star appears in a single published study, that of Aoki et al. (2007). Effective temperatures for their sample of stars were estimated using broadband photometry and the color- $T_{\text{eff}}$  relations of Alonso et al. (1999). Although  $T_{\text{eff}}$  values were

calculated using  $(V - K)$ ,  $(V - R)$ ,  $(V - I)$ , and  $(R - I)$  colors, the  $(V - K)$ -based  $T_{\text{eff}}$  were adopted for most of their sample, because  $(V - K)$  has been demonstrated to provide the best photometric  $T_{\text{eff}}$  estimate for CEMP stars (Cohen et al. 2002). The  $T_{\text{eff}}$  were then refined, and  $\log g$ ,  $\xi$ , and the Fe abundances were derived, spectroscopically. For HE 0507-1653, however, too few weak Fe I lines were present in its spectrum to allow for an accurate microturbulent velocity to be determined, so  $\xi = 2.0 \text{ km s}^{-1}$ , a value close to the average for the remaining stars in their sample, was assumed. The final stellar parameters for HE 0507-1653 from Aoki et al. (2007) and those adopted here are  $T_{\text{eff}} = 5000 \text{ K}$ ,  $\log g = 2.4$ ,  $\xi = 2.0 \text{ km s}^{-1}$ , and  $[\text{Fe}/\text{H}] = -1.38$ .

**HE 1005-1439:** Aoki et al. (2007) is also the source for the stellar parameters adopted for this star. The  $(V - K)$ -based  $T_{\text{eff}}$  for HE 1005-1439, though, was found to be  $\sim 650 \text{ K}$  higher than the average  $T_{\text{eff}}$  calculated using the  $(V - R)$ ,  $(V - I)$ , and  $(R - I)$  colors, and the authors adopted the lower  $T_{\text{eff}}$ , suspecting the  $(V - K)$ -based  $T_{\text{eff}}$  was in error. We too adopt this lower temperature,  $T_{\text{eff}} = 5000 \text{ K}$ , as well as the other parameters from the Aoki et al. study:  $\log g = 1.9$ ,  $\xi = 2.0 \text{ km s}^{-1}$ , and  $[\text{Fe}/\text{H}] = -3.17$ .

## 4.2. Model Atmospheres

The structure of a stellar photosphere is dependent in part on the star’s chemical composition due to the contribution of metals to the continuous opacity. As the concentration of metals increases, the electron pressure increases as a result of a greater number of free electrons, which in turn affects the temperature and pressure stratification of the photosphere. Metals such as C, Si, Al, Mg, and Fe contribute the most to the continuous opacity, and so the photospheres of CEMP stars, with their enhanced C abundances, are expected to have temperature and pressure profiles that differ from those of “C-normal” metal-poor stars. In light of this, using model stellar atmospheres constructed with scaled solar abundances for a chemical abundance analysis of CEMP stars is less than optimal, as the change in the temperature and pressure structure in the line-forming regions due to the enhanced C, if not properly modeled, could result in inaccurate abundance derivations.

Unfortunately, C-enhanced models are not as readily available as models with scaled solar abundances, so it is not surprising that the majority of CEMP star abundance studies found in the literature have made use of the latter. Nonetheless, a handful of these studies have addressed the use of C-enhanced models versus solar-scaled models (e.g., Lucatello et al. 2003; Aoki et al. 2007), and one study, that of Hill et al. (2000), has provided results from a more comprehensive investigation. Hill et al. compared the profiles of the temperature and the molecular partial pressures of three C-bearing molecules versus the gas pressure of a

C-enhanced model atmosphere based on the revised MARCS code (Plez et al. 1992) and two solar-scaled models, one from the grids of Kurucz (Kurucz 1992) and one from the MARCS code (Gustafsson et al. 1975), with parameters  $T_{\text{eff}} = 4500$  K,  $\log g = 1$ , and  $[\text{Fe}/\text{H}] = -3$ . They found that the temperature gradient in the C-enhanced model differed significantly from those of the solar-scaled models. The differences in the derived abundances using the different models are not quantified by the authors, but they do show that the upper layers of the C-enhanced atmosphere, where strong lines generally form, are cooler than in the C-normal atmospheres. Conversely, in the deeper layers where intermediate and weaker lines form, they showed that the C-enhanced models are hotter. These differences in the temperature structure can affect abundance derivations, especially those based on molecular features which are highly sensitive to temperature.

While a more rigorous study of metal-poor stellar atmosphere models enriched with C, as well as N and O, and their effect on stellar abundance derivations is needed, we have taken a more empirical approach to addressing the issue. We have generated both solar scaled and C-enhanced models using the adopted stellar parameters (Table 2) for each star in our sample and have used both models in our abundance analysis. The solar scaled models have been interpolated from the ATLAS9 grids of Kurucz<sup>7</sup>. These models assume local thermodynamic equilibrium (LTE) and use the convective overshoot approximation. The C-enhanced models have been generated using the LTE stellar atmosphere code ATLAS12 (Kurucz 1996). These models also include enhancements in N and O. The C and N abundances, which are given in Table 2, are from the literature: Aoki et al. (2002c) for HE 0054-2542, and Aoki et al. (2007) for HE 0507-1653 and HE 1005-1439. Oxygen abundances are not available for these stars, so we adopted an abundance of  $[\text{O}/\text{Fe}] = +0.40$ , which is typical for Galactic halo stars.

### 4.3. Abundance Derivations

The abundance analysis of the three stars in our sample has been carried out using the stellar line analysis code MOOG (Snedden 1973). Spectral synthesis was used to fit the [C I] line with the C abundance being the only free parameter. The oscillator strength for this transition,  $\log gf = -8.136$ , is taken from Allende Prieto et al. (2002), who averaged the values given by Galavis et al. (1997) and Hibbert et al. (1993). This value is in agreement with that provided by the NIST database<sup>8</sup> ( $\log gf = -8.14$ ), and it is in reasonable agreement with the value ( $\log gf = -8.21$ ) found in the Vienna Atomic Line Database (VALD;

---

<sup>7</sup>See <http://kurucz.harvard.edu/grids.html>

Piskunov et al. 1995; Kupka et al. 1999; Ryabchikova et al. 1999). The atomic linelist for the region surrounding the [C I] feature is from VALD, and it includes the blending Fe I line at 8727.10 Å ( $\log gf = -3.93$ ). Although we expect this Fe I line to be of no consequence in the spectra of our metal-poor stars, Bensby & Feltzing (2006) determined that the line can be important for stars with  $T_{\text{eff}} < 5700$  K, so for completeness, we include it in our linelist. Transition data for three CN lines in the immediate vicinity of the [C I] line are also included in the linelist and are taken from Gustafsson et al. (1999). The fits to the observed spectra are shown in Figure 1.

In addition to the  $\lambda 8727$  [C I] feature, we have scoured the bHROS spectra for additional spectral lines and have identified for each star 2–8 Fe I lines, 2–3 high-excitation C I permitted lines, 5–9 resolved CN lines of the CN red system, and the K I resonance line at 7698.96 Å. The Fe I lines provide a measurement of the overall stellar non-CNO metallicity, and our analysis provides an additional independent determination of the Fe abundances of the stars in our sample. Non-local thermodynamic equilibrium effects are expected to influence the formation of high-excitation C I lines, so the comparison of the C I-based abundances to those based on the [C I] feature provide a empirically determined estimate of the magnitude of the effect in these CEMP stars. The CN lines have been analyzed for N abundances, assuming the C abundance derived from the [C I] feature. Nitrogen abundances for CEMP stars have been largely derived from CN molecular bands at 3885 and 4215 Å via synthetic synthesis (e.g., Cohen et al. 2006; Aoki et al. 2007), so our analysis of individual CN lines of the red system provides an independent measurement of the N abundances of our sample. We note that many additional CN lines of the red system are found in our spectra, but we have concentrated on a handful of the cleanest lines that could be securely identified. Finally, potassium is predominately produced in the oxygen-burning zones of Type II supernovae (Woosley & Weaver 1995), so determining its abundance may provide some insight into the chemical history of the prenatal gas from which the stars formed. A sample of Fe I and CN features in our bHROS spectra is shown in Figure 2.

Equivalent widths of the Fe I, C I, CN, and K I lines were measured using the 1-D spectrum analysis software SPECTRE (Fitzpatrick & Sneden 1987) and were then used to derive abundances with the `abfind` driver in the MOOG package. The atomic parameters for the Fe I, C I, and K I lines were obtained from VALD. We made use of the extensive list of Davis & Phillips (1963) in the identification of measurable CN lines and have adopted the wavelengths therein; transition probabilities for the CN lines are from a proprietary list (A. McWilliam, private communication). The adopted atomic parameters and the measured

---

<sup>8</sup>See <http://physics.nist.gov/PhysRefData/ASD/index.html>

EWs for each star are listed in Table 3. In addition to EWs, SPECTRE was used to measure for each star the observed wavelengths of five lines in our linelist in order to calculate radial velocities ( $V_r$ ). The heliocentric-corrected mean values, along with the uncertainties in the means ( $\sigma_{\text{mean}} = \sigma/\sqrt{N-1}$ , where  $\sigma$  is the standard deviation and  $N$  is the number of lines measured), are provided in Table 2.

## 5. RESULTS & DISCUSSION

The results of the abundance derivations and error analysis are tabulated in Table 4. The [Fe/H] abundances, as are all relative abundances appearing herein, are given relative to the solar abundances provided by Asplund, Grevesse, & Sauval (2005a):  $A_{\odot}(\text{Fe}) = \log N_{\odot}(\text{Fe}) = 7.45$ ,  $A_{\odot}(\text{C}) = 8.39$ , and  $A_{\odot}(\text{N}) = 7.78$ . Before the derived abundances are discussed, the results of the error analysis and the comparison of the abundances derived using the C-enhanced and solar-scaled models are presented.

### 5.1. Abundance Uncertainties

The abundance uncertainties provided in Table 4 are based on abundance sensitivities of each individual element to changes in the input stellar parameters; they do not include any systematic errors, which may be considerable, resulting from assumptions made in the analysis (including the neglect of possible 3D and NLTE effects) or other potential sources. For the analysis including the solar-scaled ATLAS9 models, the parameters are  $T_{\text{eff}}$ ,  $\log g$ ,  $\xi$ , and [m/H], the overall stellar metallicity. For the analysis including the C-enhanced ATLAS12 models, in addition to the parameters previously listed, sensitivities to the model C and N abundances were also calculated. Following Aoki et al. (2007), the source of the stellar parameters adopted for HE 0507-1653 and HE 1005-1439, we assume uncertainties of  $\pm 100$  K,  $\pm 0.30$  dex, and  $\pm 0.25$  km s $^{-1}$  for  $T_{\text{eff}}$ ,  $\log g$ , and  $\xi$ , respectively. We point out, however, that Aoki et al. (2007) adopted an uncertainty of  $\pm 0.30$  km s $^{-1}$  for  $\xi$ . Uncertainties of  $\pm 0.15$  dex for [m/H],  $\pm 0.20$  dex for C, and  $\pm 0.20$  dex for N were adopted for the ATLAS12 analysis. The final abundance uncertainties ( $\sigma_{\text{Total}}$ ) are the quadratic sum of the abundance uncertainties based on the parameter sensitivities and the uncertainty in the mean abundance for species whose abundance has been derived from more than one spectral line.

The abundance sensitivities to changes in the stellar parameters of the ATLAS12 models are given for HE 0054-2542 in Table 5. The sensitivities for HE 0054-2542 are representative of those for all three stars, although some resulting uncertainties warrant special comment.

First, as is evident in Table 4, the abundance uncertainties arising from the ATLAS9 and ATLAS12 analyses do not differ greatly. While one might assume this suggests that the derived abundances are not sensitive to changes in the enhanced C abundances of the ATLAS12 models, this is not the case for the N abundances, for which a change in C abundance of  $\pm 0.50$  dex can lead to a N abundance change of  $\pm 0.13$  dex. However, because the uncertainty in the N abundances derived from the CN lines is dominated by the sensitivities to  $T_{\text{eff}}$  and  $\log g$ , the sensitivity to C does not greatly affect  $\sigma_{\text{Total}}(\text{N})$ . Second, the  $\sigma_{\text{Total}}(\text{N})$  is significantly larger than for the other elements analyzed because of the acute sensitivity of the N abundance to  $T_{\text{eff}}$  and  $\log g$ . Its sensitivity to model  $[\text{m}/\text{H}]$  and C abundance also contributes a small amount to  $\sigma_{\text{Total}}(\text{N})$ . Third, none of the other abundances derived for the three stars are sensitive to the adopted N abundance, suggesting that the N abundances do not affect significantly the structure of the ATLAS12 model atmospheres. Last, the  $\sigma_{\text{Total}}$  for the C I abundance of HE 0507-1653 is more than a factor of 1.5 larger than those of the other two stars. This is entirely due to the large uncertainty in the mean abundance, which has a standard deviation of 0.32 dex. Such a large uncertainty is not entirely surprising given that only two C I lines with vastly different line strengths (18 and 217  $\text{m}\text{\AA}$ ) were measurable for this star; the sensitivity of its C I abundance to the other parameters is comparable to those of the other stars.

## 5.2. C-Enhanced vs. Solar-Scaled Models

In Table 4, the results of both the C-enhanced ATLAS12 and solar-scaled ATLAS9 (hereafter we will simply refer to these as ATLAS12 and ATLAS9) analyses are given. The Fe, [C I], and K abundances of the three stars are consistent between the two analyses, with abundance differences being  $\leq 0.05$  dex. There are greater discordances, however, between the ATLAS12 and ATLAS9 abundances for C I and N. The differences are such that the ATLAS12 C I abundances are 0.09 – 0.14 dex lower than the ATLAS9 abundances, whereas the ATLAS12 N abundances are consistently higher than those from the ATLAS9 analysis by 0.15 dex.

The differences in the C I and N abundances, as well as the minor discrepancies in the Fe, [C I], and K abundances, are entirely attributable to the divergences in the temperature and pressure structures of the ATLAS12 and ATLAS9 model atmospheres. In Figures 3 – 5, temperature is plotted versus the logarithm of the pressure from the ATLAS12 and ATLAS9 models of HE 0054-2542, HE 0507-1653, and HE 1005-1439, respectively. In each figure, the optical depths<sup>9</sup> at reference wavelength 5000  $\text{\AA}$  ( $\tau_{5000}$ ) that bracket the line forming regions of the spectral features included in our analysis are marked; the inset included with each figure

highlights the temperature- $\log P_{\text{gas}}$  relations of these regions. As can be seen in the figures, the ATLAS12 model is hotter than the ATLAS9 model in the line forming region of each star except at the deepest boundaries for HE 0054-2542 and HE 1005-1439, the two most Fe-deficient stars, where the ATLAS12 model dips below the ATLAS9 model. Quantifying accurately the effect of the model differences on the abundances derived from each spectral line is difficult due to the convolution of the effects of the temperature and pressure differences at a given  $\tau_{5000}$ , but the differences of the models at the mean depths of formation for each line are such that they qualitatively account for the abundance discrepancies that are seen. For example, the mean depths of formation of the C I lines differ between the models in such a way that the ATLAS9 temperature at this layer is less than the ATLAS12 temperature and conversely, the ATLAS9 pressure is greater than the ATLAS12 pressure. Both of these differences conspire to result in an ATLAS9 abundance that is greater than the ATLAS12 one, which is seen for all three stars.

*The differences in the ATLAS12 and ATLAS9 abundances of C I and N demonstrate that model atmospheres characterized by metal abundances scaled from the solar composition are not ideally suited for chemical abundance analyses of CEMP stars.* This result corroborates the conclusion of Hill et al. (2000). The comparison of their C-enhanced and solar-scaled models are similar to those seen here for the two most Fe-deficient stars HE 0054-2542 and HE 1005-1439: the C-enhanced model is hotter at a given pressure than the solar-scaled model in the deepest atmospheric layers, and it is cooler in the outer layers. Hill et al. point out that very strong lines, such as the molecular band heads, would be stronger in the C-enhanced model because of the lower temperature in the outer regions in which these lines are expected to form, and that the intermediate and weak lines that form deeper in the atmospheres, near  $\log \tau_{5000} = -1$ , will be weaker in the C-enhanced models due to their higher temperatures in these layers. Because of these structural differences, Hill et al. conclude that C-enhanced models should be used in analyses of CEMP stars if possible.

As stated above, accurately quantifying the effect of using solar-scaled as opposed to C-enhanced model atmospheres in abundance analyses of CEMP stars is challenging. The differences in the derived abundance for any given element are dependent on both the structural differences in the temperature and pressure profiles of the model atmospheres and the depth of formation of each individual spectral line. This is evident by the differing results for Fe, [C I], and K, which show no or only minor differences in the ATLAS12 and ATLAS9 abundances, and for C I and N, which show more significant discrepancies. The magnitude of the effect is expected to be even more severe for the molecular band heads, which are highly

---

<sup>9</sup>The  $\tau_{5000}$  values have been taken from the output files of the MOOG package and represent the optical depths of the mean depth of formation for each spectral line.

sensitive to temperature and pressure, that are often used in the derivation of C, N, and O abundances of CEMP stars. Any inaccuracies in the derived abundances of CEMP stars will negatively affect the interpretation of the nucleosynthetic history of these stars and their role in the chemical evolution of the Galaxy. Under the assumption that C-enhanced models more accurately represent the real atmospheres of CEMP stars, it is clear that C-enhanced models should be used in their abundance analyses. Moreover, we hope our analysis will provide sufficient motivation for a more rigorous examination of C-enhanced model atmospheres and their effect on the derived abundances of CEMP stars.

Unless explicitly stated to the contrary, the remaining discussion will refer to the abundances derived using the C-enhanced ATLAS12 models.

### 5.3. Abundances

#### 5.3.1. Iron Abundances

The limited wavelength coverage of the bHROS spectra and the Fe deficiency of the stars in our sample combine to restrict the number of lines ( $N \leq 8$ ) from which Fe abundances can be derived for each star. For the two most Fe-deficient stars, HE 0054-2542 and HE 1005-1439, only three and two Fe lines, respectively, were measurable. Regardless, the derived Fe abundances of all three stars (Table 4) are in very good agreement with previously determined values. Preston & Sneden (2001) and Aoki et al. (2002c) have both analyzed HE 0054-2542 and have found respectively  $[\text{Fe}/\text{H}] = -2.67$  and  $[\text{Fe}/\text{H}] = -2.64$ ; our value of  $[\text{Fe}/\text{H}] = -2.66 \pm 0.08$  falls between their results. Our abundances of  $[\text{Fe}/\text{H}] = -1.42 \pm 0.15$  for HE 0507-1653 and  $[\text{Fe}/\text{H}] = -3.08 \pm 0.13$  for HE 1005-1439 are in good agreement with those of Aoki et al. (2007), who derived  $[\text{Fe}/\text{H}] = -1.38$  for the former and  $[\text{Fe}/\text{H}] = -3.17$  for the latter. Thus, despite utilizing different spectral lines and different model atmospheres, our results confirm the subsolar Fe abundances of HE 0054-2542, HE 0507-1653, and HE 1005-1439.

#### 5.3.2. C Abundances from the [C I] Line

As shown in Figure 1, the synthetic spectra of the  $\lambda 8727$  region fit well the observed spectra of each star. The resulting abundances from the best fits of the [C I] features are given in Table 4. Adopting our derived  $[\text{Fe}/\text{H}]$  abundances and  $A_{\odot}(\text{C}) = 8.39$ , the C abundances relative to Fe are listed in Table 6 and are  $[\text{C}/\text{Fe}] = +2.12 \pm 0.14$  for HE 0054-2542,  $[\text{C}/\text{Fe}] = +1.33 \pm 0.21$  for HE 0507-1653, and  $[\text{C}/\text{Fe}] = +2.14 \pm 0.17$  for HE 1005-1439,

where the stated uncertainty is the quadratic sum of the C and Fe uncertainties given in Table 4. We discuss the abundances for each star in turn.

**HE 0054-2542:** similar to the [Fe/H] abundance, our [C/Fe] ratio from the 1D LTE analysis for this star is bracketed by the abundances derived by Preston & Sneden (2001) and Aoki et al. (2002c), and it is in good agreement with both of their values. Preston & Sneden found an abundance of [C/Fe] = +2.2 by analyzing the CH bands at wavelengths 4228 – 4241 Å and 4358 – 4374 Å. Their derived abundance is labeled as uncertain, although the uncertainty is not quantified. The abundance from Aoki et al., [C/Fe] = +2.0, is derived from the (1-0) band of the C<sub>2</sub> Swan system at 4735 Å, and the result is also given without an uncertainty estimate. Typical errors in [C/Fe] abundances derived from high-resolution spectra range from about 0.15 to 0.25 dex (e.g., Cohen et al. 2006; Sivarani et al. 2006), and if this typical uncertainty is adopted for the Preston & Sneden and Aoki et al. studies, their C abundances are in agreement. Both of the previously derived abundances are within the uncertainty associated with our value derived from the [C I] feature, and we thus conclude that the three measurements are consistent.

**HE 0507-1653:** the [C I]-based 1D LTE abundance for this star is in excellent agreement with the value found by Aoki et al. (2007), the difference between the two results being only 0.04 dex. Aoki et al. derived an abundance of [C/Fe] = +1.29 ± 0.19 based on an analysis of the C<sub>2</sub> Swan (0-1) band at 5635 Å. The (0-1) band was chosen for measurement, because, according to the authors, the CH G-band and the C<sub>2</sub> Swan (0-0) band at 5170 Å were saturated and not suitable for the purpose.

**HE 1005-1439:** unlike for the two more Fe-abundant stars in our sample, the 1D LTE-based C abundance derived from the [C I] feature for HE 1005-1439 differs from the previously determined measurement. This star was analyzed by Aoki et al. (2007) as part of the same study that included HE 0507-1653, although the abundance for HE 1005-1439 is based on the C<sub>2</sub> Swan (0-0) band at 5170 Å instead of the (0-1) band at 5635 Å. Aoki et al. derived an abundance of [C/Fe] = +2.48 ± 0.20, which is 0.34 dex, or about a 2σ deviation, larger than our [C I]-based abundance. Aoki et al. (2007) suggest that C abundances derived from C<sub>2</sub> bands may be systematically higher by 0.2 dex than those derived from CH bands based on the results of Aoki et al. (2002d), who derived consistent C abundances for the CEMP star LP 625-44 from the (1-0), (0-0), and (0-1) bands of the Swan system but found the abundance derived using the CH band at 4323 Å to be about 0.20 dex lower. However, the abundances derived for HE 0054-2542 do not support the existence of such a systematic offset; indeed, the C<sub>2</sub>-based abundance derived for this star by Aoki et al. (2002c) is 0.2 dex *lower* than the CH-based abundance derived by Preston & Sneden (2001), in direct contrast to the suggested systematic offset. Furthermore, a similar offset has not been suggested to exist

between individual lines of the C<sub>2</sub> Swan system. On the contrary, Aoki et al. (2002d) find consistent results from three different C<sub>2</sub> band heads using the same line list as Aoki et al. (2007). Thus, there is no reason to believe that any one of the C<sub>2</sub> Swan lines is superior to any of the others for abundance analyses and that the 0.34 dex difference in the C<sub>2</sub> and [C I]-based abundances derived for HE 1005-1439 is due to the particular C<sub>2</sub> Swan line used.

Because the [C I] and C<sub>2</sub>-based abundances for HE 1005-1439 differ at about the  $2\sigma$  level of the internal uncertainty, the difference cannot be ascribed with statistical confidence to the inability of the C<sub>2</sub> Swan lines to reproduce reliable LTE abundances. Instead, the abundance difference may be a result of other inadequacies in either of the abundance analyses, although the exact component of the analyses that could be responsible for such a large discrepancy is not readily identifiable. As discussed above, the adopted linelists and the modeling of the lines do not seem to be at fault. The stellar parameters used by Aoki et al. (2007) are the same as those used in our analysis, so while the sensitivity of the abundance derived from the  $\lambda 5170$  C<sub>2</sub> line to changes in stellar parameters may differ from that of the [C I]-based abundance, it is unlikely the adopted stellar parameters can account for the 0.34 dex difference in the derived C abundance. Despite the moderate S/N = 65 of the coadded spectrum for HE 1005-1439, the [C I] line is well shaped and easily identifiable (Figure 1), and an excellent fit with the synthetic spectrum to both the continuum and the [C I] feature is obtained. Furthermore, to reproduce the [C/Fe] abundance of HE 1005-1439 derived by Aoki et al. (2007) would require an equivalent width that is approximately a factor of two larger than the one measured in our bHROS spectrum (Figure 6). Thus, while the spectrum of HE 1005-1439 is of slightly lower quality than those of the other two stars in our sample, there is no conspicuous evidence to suggest that it is a source of significant error in the derived C abundance.

Having largely ruled out other possibilities, in § 5.4 we discuss whether 3D effects could explain the different abundance results from the [C I] and C<sub>2</sub> lines.

### 5.3.3. *The High-Excitation C I Lines*

Carbon abundances have been derived from high-excitation (7.48 – 8.77 eV) C I lines in the spectra of our CEMP star sample for comparison to the [C I] results. The C I lines are known to form out of LTE, and the measurements presented here should provide an empirical estimate of the associated NLTE effects in these stars. The comparison of the 1D LTE abundances derived from the [C I] and C I lines is made in Table 7, and as expected from existing NLTE calculations (Fabbian et al. 2006), the abundances based on the C I lines are greater than those derived from the forbidden line. Similarly, Aoki et al.

(2002d) derived the C abundance of the CEMP star LP 625-44 from five high-excitation C I lines and found the abundance to be 0.45 dex greater than that derived from CH and C<sub>2</sub> molecular features. The stellar parameters of LP 625-44 ( $[\text{Fe}/\text{H}] = -2.7$ ,  $[\text{C}/\text{Fe}] = +2.25$ ,  $T_{\text{eff}} = 5500$  K, and  $\log g = 2.5$ ; Aoki et al. 2002d) are similar to those of HE 0054-2542, and the C I overabundances are nearly identical for the two stars. In § 5.4, we present predicted NLTE abundances for C I and the corresponding 3D effects for [C I] .

#### 5.3.4. Nitrogen Abundances

Numerous lines of the CN red system are present in our bHROS spectra, and we have identified 5 – 9 clean, resolved lines for each star (Table 3) suitable for abundance analysis. The mean abundances derived from these lines are provided in Table 4 and correspond to relative abundances of  $[\text{N}/\text{Fe}] = +1.24 \pm 0.35$  (0.03) for HE 0054-2542,  $[\text{N}/\text{Fe}] = +1.20 \pm 0.34$  (0.02) for HE 0507-1653, and  $[\text{N}/\text{Fe}] = +2.27 \pm 0.35$  (0.09) for HE 1005-1439 (Table 6). The number given in the parentheses following each uncertainty is the standard deviation in the mean abundance for each star and is indicative of the excellent agreement in the line-by-line abundances derived from the CN red system features. As mentioned above in §5.1, the large uncertainties in the N abundances arise from the severe sensitivity of these molecular features to changes in the  $T_{\text{eff}}$  and  $\log g$  parameters and are typical compared to those from other studies (Cohen et al. 2006; Aoki et al. 2007).

Previous N abundance determinations for the three stars in our sample have all been based on features of the CN blue system near 3880 and 4215 Å and are all at least 0.40 dex lower than the abundances presented here. Preston & Sneden (2001) and Aoki et al. (2002c) both derived N abundances for HE 0054-2542 from the 3880 Å CN band and found  $[\text{N}/\text{Fe}] = +0.7$  and  $+0.3$ , respectively. Aoki et al. (2002b) revisited the analysis of Aoki et al. (2002c) and determined the  $\lambda 3880$  CN band was too strong in their spectrum to provide an accurate abundance estimate. Using the  $\lambda 4215$  CN band, Aoki et al. (2002b) derived an abundance of  $[\text{N}/\text{Fe}] = +0.8$ , a value that is in better agreement with that of Preston & Sneden but lower by 0.44 dex than our derived abundance. The N abundances for HE 0507-1653 and HE 1005-1439 have been determined by Aoki et al. (2007) from an analysis of the  $\lambda 4215$  CN band for each star. Their reported abundances are  $[\text{N}/\text{Fe}] = +0.80$  for the former and  $[\text{N}/\text{Fe}] = +1.79$  for that latter; these values are 0.40 and 0.48 dex, respectively, lower than our abundances.

Given the large uncertainties in the N abundances, the differences between our values and those previously published cannot be said to be statistically significant. Nonetheless, the disagreement is striking. About 50% of the difference for each star is attributable to

our use of the C-enhanced ATLAS12 model atmospheres, the abundances from which are a consistent 0.15 dex higher than those derived from the solar-scaled ATLAS9 analysis. The N abundances from our ATLAS9 analysis are  $\sim 0.3$  dex higher than the literature values, and the source of this remaining difference is not so obvious. The adoption of different molecular dissociation energies by different studies can lead to diverging abundances, but this is not the case here. Following Spite et al. (2005) and Norris et al. (2007), we have adopted a dissociation energy of  $D_0 = 7.76$  eV for the CN molecule, which is essentially the same as the value of  $D_0 = 7.75$  eV adopted by Aoki et al. (2002b) and Aoki et al. (2007)<sup>10</sup>. Spite et al. (2005) derived the N abundances of 10 metal-poor giants from both the CN blue band near 3880 Å and the NH band at 3360 Å, and the CN-based abundances were found to be systematically lower by  $\sim 0.40$  dex than the NH-based abundances. The reason for the discrepancy was not apparent to the authors, but we find it to be similar to the  $\sim 0.30$  dex difference between the CN blue bands and CN red system abundances from the ATLAS9 analysis seen here. Taken together, the results of Spite et al. (2005) and of our study suggest that analyses of the CN blue system bands underestimate the N abundances of metal-poor giants. Because the CN band is used often for the derivation of N abundances in such stars, further investigation into the ability of this feature to provide accurate abundances is needed.

Accurately determined N abundances are critical to understanding the nucleosynthetic history of CEMP stars and to placing constraints on stellar evolution models. Mass-transfer from a primary companion during its asymptotic giant branch (AGB) phase is thought to be the source of the enhanced C and the enhancements of other elements in the photospheres of the majority of CEMP stars (Ryan et al. 2005). Intermediate mass AGB stars (initial masses of  $\sim 4 - 6 M_\odot$ ) are predicted to be efficient producers of primary N (Herwig 2004), and it has been suggested that N-rich counterparts to CEMP stars, Nitrogen-Enhanced Metal-Poor (NEMP) stars, should also be common in the Galactic halo (Johnson et al. 2007). The initial survey of 21 CEMP stars by Johnson et al. was carried out using ATLAS9 models with solar-scaled abundances, and their analysis of the NH band head near 3360 Å produced no identified NEMP stars. Given the 0.15 dex difference between the N abundances derived here using the ATLAS12 and ATLAS9 atmospheric models, an investigation of the effect of CNO-enhanced model atmospheres of potential NEMP stars on derived N abundances is warranted. Otherwise, *bona fide* NEMP stars may not be identified.

---

<sup>10</sup>The CN dissociation energy does not appear in the published papers of Aoki et al. and has been provided via private communication.

### 5.3.5. Potassium Abundances

Potassium abundances have been determined for large samples of metal-poor stars by a handful groups, starting with Gratton & Sneden (1987) and then more recently by Cayrel et al. (2004), Zhang & Zhao (2005), and Zhang et al. (2006). The consensus among these studies is that the LTE  $[K/Fe]$  ratios for metal-poor stars, irrespective of evolutionary state, are super-solar, and they evince substantial scatter, particularly at metallicities of  $[Fe/H] \leq -1.0$ . The K I resonance line at 7699 Å, generally the only line available in the spectra of late-type stars with which K abundances can be derived, is highly sensitive to NLTE effects, and large negative corrections (-0.2 to -0.8 dex) for LTE abundances derived from this line have been predicted (Takeda et al. 2002). The magnitude of the corrections have been shown to be dependent on  $T_{\text{eff}}$  and  $\log g$  but not  $[Fe/H]$ , and after applying the corrections to the LTE abundances, the super-solar  $[K/Fe]$  ratios and the large scatter remain (e.g., Takeda et al. 2002; Zhang & Zhao 2005).

The LTE K abundances derived for the three stars in our sample are given in Table 4 and correspond to  $[K/Fe]$  relative abundances of +0.61, +0.74, and +0.50 for HE 0054-2542, HE 0507-1653, and HE 1005-1439, respectively. The K abundance has been derived for only one other CEMP star, HE 1410-0004 (Cohen et al. 2006), a subgiant with  $[Fe/H] = -3.02$ ; the K abundance for this star has been determined to be  $[K/Fe] = +0.71$ . The LTE abundances of these CEMP stars fall squarely among the scatter in the LTE  $[K/Fe]$  abundances seen for C-normal metal-poor stars (e.g., Cayrel et al. 2004; Zhang & Zhao 2005). The consistent abundances derived using the C-enhanced ATLAS12 and solar-scaled ATLAS 9 models and the lack of a metallicity dependence on the calculated NLTE corrections both suggest that the NLTE effects associated with K abundances in CEMP stars do not differ significantly from those in C-normal stars. While targeted K NLTE calculations for CEMP stars are needed, the existing NLTE corrections to K abundances should, to first approximation, be adequate.

## 5.4. 3D AND NLTE EFFECTS

The elemental abundances presented in § 5 were estimated based on 1D model atmospheres and LTE spectral line formation. Since these may be questionable assumptions especially in the low-density regimes of metal-poor red giant atmospheres (Asplund 2005), it is important to investigate the possible systematic errors introduced in the analysis by these simplifications. Indeed, the difference in the HE 1005-1439 C abundances derived from  $[C\text{ I}]$  and molecular lines, and the systematically lower abundances derived from  $[C\text{ I}]$  compared with C I for the 1D LTE analysis may signal exactly such 3D and/or NLTE effects.

Three-dimensional time-dependent hydrodynamical model atmospheres have relatively recently started to be employed for abundance analysis of metal-poor stars (e.g. Asplund et al. 1999; Asplund & García Pérez 2001; Asplund 2005; Asplund et al. 2006; Collet et al. 2006, 2007; González Hernández et al. 2008). The main difference in the atmospheric structure is much lower temperatures in the line-forming region of the 3D model compared with classical 1D model atmospheres; these temperature differences affect in particular abundances derived from molecular lines, neutral species, and low-excitation lines (Asplund et al. 1999). C I is a majority species and hence is less affected by temperature variations than, for example, Li I or Fe I, but because the  $\lambda 8727$  [C I] line originates from a relatively low-excitation level (1.26 eV), one would expect the 1D abundances to be slightly overestimated at the lowest metallicities (Asplund 2005).

We have carried out 3D LTE line formation calculations for the [C I] 8727 Å transition using the same 3D hydrodynamical model atmospheres as described in Collet et al. (2007), which have similar stellar parameters as our three stars in terms of  $T_{\text{eff}}$ ,  $\log g$  and [Fe/H]. The 3D models were constructed assuming scaled solar abundances and are thus not directly applicable to CEMP stars. For an exploratory study like this we nevertheless consider this a justifiable approach. Because the 3D effects are estimated from a differential comparison with 1D MARCS models (Asplund et al. 1997) computed assuming identical stellar parameters, including the chemical composition, to first-order the effects of a C-enriched atmosphere discussed in § 5.2 will cancel out. Specifically constructed 3D models appropriate for CEMP stars would be valuable, however, for more accurate estimates of the various 3D effects. We also note that a comparison with MARCS models is more relevant than with Kurucz models, because the 3D and MARCS models are built on the same microphysics in terms of opacities and equation-of-state.

The  $\lambda 8727$  [C I] 3D line formation calculations have been computed for metallicities of [Fe/H] = +0, -1, -2, and -3, and the 3D abundance effects appropriate for our three stars have been estimated and applied to the 1D LTE results described in § 5.3. The 3D-based abundances are given in Table 6. As expected, the 3D effects remain modest for the [C I] line: slightly positive for HE 0507-1653 and  $\sim -0.1$  dex for HE 0054-2542 and HE 1005-1439, the two most metal-poor stars. In this respect, [C I] behaves like lines from other majority species such as O I (Asplund 2005; Collet et al. 2007), but the 3D effects are less severe than for example for the [O I] 6300 Å line for a given line strength because of its higher excitation potential. It should be noted that the exact value of the 3D corrections remains somewhat uncertain since the O abundances are not yet known in these stars; if [O/Fe] is significantly larger than the +0.4 assumed here, a greater fraction of C will be tied up in CO. This notwithstanding, it is clear that the 3D effects on the  $\lambda 8727$  [C I] line will remain relatively small.

Fabbian et al. (2006) have investigated the line formation of neutral C atoms in late-type stars and have provided predicted NLTE abundance corrections for the high-excitation C I lines employed here for stars characterized by a range of  $T_{\text{eff}}$ ,  $\log g$ , and metallicities. The NLTE abundance corrections for HE 0054-2542, HE 0507-1653, and HE 1005-1439 are  $-0.30$ ,  $-0.45$ , and  $-0.30$  dex, respectively, when assuming a C abundance enhancement of  $[\text{C}/\text{Fe}] = +0.4$  and neglecting the highly uncertain inelastic H collisions (Asplund 2005). Thus, NLTE effects on the C I lines can explain most of the differences between the abundances derived from the C I and [C I] lines. We note that Fabbian et al. indeed predict that the magnitude of the C I NLTE corrections should become larger with increasing  $[\text{C}/\text{Fe}]$ , because the line-formation is then shifted outwards in the atmosphere where the departures from LTE are more pronounced. This effect has not been investigated computationally for C enhancements of  $[\text{C}/\text{Fe}] > 0.4$ , and our result, combined with that of Aoki et al. (2002d), suggests that such a study is very much needed. Additionally, the 3D NLTE line formation for C I has not yet been studied due to computational challenges arising from the large number of atomic levels needed to be considered, but given the very substantial 1D NLTE effects uncovered here, such calculations would also be very welcome.

As is clear from Table 6, taking 3D and NLTE effects into account for [C I] and C I, respectively, have brought the two abundance indicators into better agreement, from a difference of  $\sim 0.5$  dex to  $\sim 0.25$  dex. The remaining difference can be plausibly attributed to underestimated 3D and NLTE effects, erroneous  $T_{\text{eff}}$ , or simply observational uncertainties. Of the two abundance indicators, we consider the [C I]-based abundances to be the most reliable.

As discussed in § 5.3, the abundances of HE 0054-2542 and HE 0507-1653 derived from the [C I] line are in good agreement with those derived from CH and C<sub>2</sub> features. Collet et al. (2007) have shown that, assuming scaled-solar abundances, the 3D corrections for CH are relatively constant at  $\sim -0.1$  to  $\sim -0.2$  dex down to  $[\text{Fe}/\text{H}] = -2$  for giants; C<sub>2</sub> lines were not investigated. These 3D effects would therefore not be expected to ruin the overall agreement for the two CEMP stars. More noteworthy, the C<sub>2</sub>-based abundance for HE 1005-1439 from Aoki et al. (2007) is 0.34 dex larger than our 1D result for [C I] and 0.49 dex larger than the corresponding 3D value. While no 3D calculations for C<sub>2</sub> have been performed to date, at least qualitatively this is in line with our expectations that the 3D corrections for molecular lines become more severe towards lower metallicities (Asplund & García Pérez 2001; Asplund 2005; Collet et al. 2007). Unfortunately, we are unable here to carry out such a study without a better knowledge of the stellar O abundances; the cool outer atmospheric layers of the low-metallicity 3D models that give rise to the C<sub>2</sub> lines are particularly conducive to CO molecule formation, which locks up a significant fraction of C and thereby limits the amount available for C<sub>2</sub> (the [C I] lines will be less affected by the CO formation since they

form in deeper atmospheric layers where the temperatures are significantly higher).

## 6. CONCLUSIONS

An investigation into the accuracy of published C abundances as derived from the traditionally used CH and C<sub>2</sub> Swan bands of CEMP stars has been presented. We have analyzed the  $\lambda 8727$  [C I] line, a normally reliable C abundance indicator that is impervious to NLTE effects, in high-quality Gemini-S/bHROS spectra of three CEMP stars and have compared the C abundances derived from this line to previously published values. The 1D LTE abundances derived from the [C I] feature are found to confirm the abundances derived from both CH and C<sub>2</sub> molecular features in the two most Fe-abundant stars, HE 0054-2542 and HE 0507-1653 ([Fe/H] =  $-2.66$  and  $-1.42$ , respectively), but the [C I]-based abundance of the most Fe-deficient star, HE 1005-1439 ([Fe/H] =  $-3.08$ ), is 0.34 dex, or about a  $2\sigma$  deviation, lower than the abundance derived from the C<sub>2</sub> Swan (0-0) band at 5170 Å.

As described in §5.3.2, the specific C<sub>2</sub> Swan band used to derive C abundances does not appear to be a factor in the difference seen for HE 1005-1439. Also, no particular component of the two abundance analyses could be identified as the most likely source of the discordance, although internal errors may yet be the underlying cause. Unidentified systematic errors in the analyses also cannot be ruled out as the source of the difference, but the agreement in the abundances of HE 0507-1653 derived by us and Aoki et al. (2007), the study that also derived the discordant abundance of HE 1005-1439, suggests that no such systematic errors are to be expected. Thus, the difference in the C abundance seen between the two studies may indeed be the result of 3D effects in the analysis of the C<sub>2</sub> Swan band. Collet et al. (2007) investigated the impact of 3D effects on CNO abundances of red giants derived from weak CH, NH, and OH lines and found the 3D C abundances to be 0.5 to 0.8 dex lower (for stars with [Fe/H] =  $-3.0$ ) than those derived using traditional 1D analyses. While these corrections are larger than the difference between the C<sub>2</sub> and [C I]-based abundances for HE 1005-1439, it must be pointed out that Collet et al. considered stars with *scaled-solar* metallicities, and the corrections may not be applicable to CEMP stars. Also, the 3D corrections for CH lines are not necessarily similar to those for C<sub>2</sub> lines (e.g., Asplund et al. 2005b; Collet et al. 2006).

To investigate the potential 3D effects on [C I]-based abundances of low-metallicity stars, we have carried out 3D LTE line formation calculations for [C I] using the same 3D hydrodynamical model atmospheres as described by Collet et al. (2007). The 3D correction for HE 0507-1653 is estimated to be slightly positive (+0.03 dex), while the corrections for HE 0054-2542 and HE 1005-1439 are negative ( $-0.07$  and  $-0.15$  dex, respectively). Thus,

the corrections are quite modest but do increase in magnitude at lower metallicities, similar to what is seen for the [O I] line (Asplund 2005; Collet et al. 2007). While more accurate [C I] 3D corrections for these CEMP stars await C-enhanced 3D models and more certain O abundances, the observations and calculations presented here are qualitatively in line with expectations that the 3D corrections for molecular line-based C abundances become more severe towards lower metallicities.

We have also determined abundances from high-excitation C I lines and found them to be systematically higher than the [C I]-based abundances by  $\sim 0.5$  dex when assuming LTE. One-dimensional abundance corrections have been taken from Fabbian et al. (2006), who performed NLTE calculations for a range of stellar parameters assuming a C abundance enhancement of  $[C/Fe] = +0.4$ , and the NLTE-corrected C I abundances are in significantly better agreement with the 3D [C I]-based values. However, there remains a  $\sim 0.25$  dex difference in the two C abundances which can be tentatively attributed to underestimated NLTE effects on the C I line because calculations for  $[C/Fe] > +0.4$ , which are appropriate for our sample, have not been investigated, or possibly erroneous  $T_{\text{eff}}$  values.

At this time, the complicated 3D and NLTE effects that may impact [C I], C I, CH, and C<sub>2</sub> features in the spectra of CEMP stars have not yet been fully established. Analyses of the [C I] line in high-resolution spectra of additional CEMP stars, particularly those at the lowest metallicities, for which CH and/or C<sub>2</sub>-based abundances exist or are forthcoming are needed to determine if abundances derived from the forbidden line diverge in a systematic way from those derived from the molecular features. Additionally, 3D models and NLTE line formation calculations with chemical compositions appropriate for CEMP stars are clearly needed to complement the observations. These measures are necessary so that the most accurate C abundances possible can be derived for CEMP stars.

Support for S.C.S. has been provided by the NOAO Leo Goldberg Fellowship; NOAO is operated by the Association of Universities for Research Astronomy (AURA), Inc., under a cooperative agreement with the National Science Foundation. K.C. and V.V.S. acknowledge support from the National Science Foundation (NSF) under grant AST 06-46790. T.C.B. and T.S. acknowledge partial support for this work from the NSF under grants AST 04-06784, AST 07-07776, and PHY 02-16783; Physics Frontier Center/Joint Institute for Nuclear Astrophysics (JINA). We thank W. Aoki for providing the CN molecule dissociation energy that was used in his studies. This paper is based on observations obtained with the bHROS optical spectrograph and the Gemini Observatory, which is operated by AURA, Inc., under a cooperative agreement with the NSF on behalf of the Gemini partnership: the National Science Foundation (United States), the Science and Technology Facilities Council (United Kingdom), the National Research Council (Canada), CONICYT (Chile), the Aus-

tralian Research Council (Australia), Ministério da Ciência e Tecnologia (Brazil) and SECYT (Argentina). The observations were conducted under Gemini program GS-2006B-DD-96.

*Facility:* Gemini:South (bHROS)

## REFERENCES

- Akerman, C. J., Carigi, L., Nissen, P. E., Pettini, M., & Asplund, M. 2004, *A&A*, 414, 931
- Allende Prieto, C., Lambert, D. L., & Asplund, M. 2002, *ApJ*, 573, L137
- Alonso, A., Arribas, S., & Martínez-Roger, C. 1999, *A&AS*, 140, 261
- Aoki, W., Beers, T. C., Christlieb, N., Norris, J. E., Ryan, S. G., & Tsangarides, S. 2007, *ApJ*, 655, 492
- Aoki, W., Norris, J. E., Ryan, S. G., Beers, T. C., & Ando, H. 2002a, *ApJ*, 567, 1166
- Aoki, W., Norris, J. E., Ryan, S. G., Beers, T. C., & Ando, H. 2002b, *PASJ*, 54, 933
- Aoki, W., Ryan, S. G., Norris, J. E., Beers, T. C., Ando, H., & Tsangarides, S. 2002c, *ApJ*, 580, 1149
- Aoki, W., et al. 2002d, *PASJ*, 54, 427
- Asplund, M. 2005, *ARA&A*, 43, 481
- Asplund, M. & García Pérez, A. E. 2001, *A&A*, 372, 601
- Asplund, M., Gustafsson, B., Kiselman, D., & Eriksson, K. 1997, *A&A*, 318, 521
- Asplund, M., Nordlund, Å., Trampedach, R., & Stein, R.F. 1999, *A&A*, 346, L17
- Asplund, M., Grevesse, N., & Sauval, A. J. 2005a, in *ASP Conf. Ser. 336, Cosmic Abundances as Records of Stellar Evolution and Nucleosynthesis*, ed. T. Barnes & F. Bash (San Francisco:ASP), 25
- Asplund, M., Grevesse, N., Sauval, A. J., Allende Prieto, C., & Blomme, R. 2005b, *A&A*, 431, 693
- Asplund, M., Lambert, D. L., Nissen, P. E., Primas, F., & Smith, V. V. 2006, *ApJ*, 644, 229
- Beers, T. C. 1999, in *ASP Conf. Ser. 165, The Third Stromlo Symposium: The Galactic Halo*, eds. B. K. Gibson, R. S. Axelrod, & M. E. Putman (San Francisco: ASP), 202
- Beers, T. C. & Christlieb, N. 2005, *ARA&A*, 43, 531
- Beers, T. C., Preston, G. W., & Shectman, S. A. 1985, *AJ*, 90, 2089
- Beers, T. C., Preston, G. W., & Shectman, S. A. 1992, *AJ*, 103, 1987

- Beers, T. C., et al. 2007, *ApJS*, 168, 128
- Bensby, T. & Feltzing, S. 2006, *MNRAS*, 367, 1181
- Cayrel, R., et al. 2004, *A&A*, 416, 1117
- Christlieb, N. 2003, *Rev. Mod. Astron.*, 16, 191
- Cohen, J. G., Christlieb, N., Beers, T. C., Gratton, R., & Carretta, E. 2002, *AJ*, 124, 470
- Cohen, J. G., et al. 2005, *ApJ*, 633, L109
- Cohen, J. G., et al. 2006, *AJ*, 132, 137
- Collet, R., Asplund, M., & Trampedach, R. 2006, *ApJ*, 644, L121
- Collet, R., Asplund, M., & Trampedach, R. 2007, *A&A*, 469, 687
- Davis, S. P. & Phillips, J. G. 1963, *Berkeley Analyses of Molecular Spectra* (Berkeley: Univ. of California Press)
- Fabbian, D., Asplund, M., Carlsson, M., & Kiselman, D. 2006, *A&A*, 458, 899
- Fitzpatrick, M. J. & Sneden, C. 1987, *BAAS*, 19, 1129
- Frebel, A., et al. 2006, *ApJ*, 652, 1585
- Frebel, A., Norris, J. E., Aoki, W., Honda, S., Bessell, M. S., Takada-Hidai, M., Beers, T. C., & Christlieb, N. 2007, *ApJ*, 658, 534
- Galavis, M. E., Mendoza, C., & Zeppen, C. J. 1997, *A&AS*, 123, 159
- González Hernández, J. I. , Bonifacio, P., Ludwig, H.-G. et al. 2008, *A&A*, 480, 233
- Gratton, R. G. & Sneden, C. 1987, *A&A*, 178, 179
- Green, E. M., Demarque, P., & King, C. R. 1987, *The Revised Yale Isochrones and Luminosity Functions* (New Haven: Yale Univ. Obs.)
- Gustafsson, B., Bell, R. A., Eriksson, K., & Nordlund, A. 1975, *A&A*, 42, 407
- Gustafsson, B., Karlsson, T., Olsson, E., Edvardsson, B., & Ryde, N. 1999, *A&A*, 342, 426
- Herwig, F. 2004, *ApJ*, 605, 425
- Hibbert, A., Biemont, E., Godefroid, M., & Vaeck, N. 1993, *A&AS*, 99, 179

- Hill, V., et al. 2000, *A&A*, 353, 557
- Johnson, J. A., Herwig, F., Beers, T. C., & Christlieb, N. 2007, *ApJ*, 658, 1203
- Kupka, F., Piskunov, N., Ryabchikova, T. A., Stempels, H. C., & Weiss, W. W. 1999, *A&AS*, 138, 119
- Kurucz, R.L. 1992, in *IAU Symp.* 149, ed. B. Barbury & A. Renzini, (Dordrecht:Kluwer), 225
- Kurucz, R.L. 1996, in *IAU Symp.* 176, ed. K.G. Strassmeier & J.L. Linsky, (Dordrecht:Kluwer), 523
- Lambert, D. L. 1978, *MNRAS*, 182, 249
- Lambert, D. L. & Swings, J. P. 1967, *Sol. Phys.*, 2, 34
- Lucatello, S., Gratton, R., Cohen, J. G., Beers, T. C., Christlieb, N., Carretta, E., & Ramírez, S. 2003, *AJ*, 125, 875
- Lucatello, S., Beers, T. C., Christlieb, N., Barklem, P. S., Rossi, S., Marsteller, B., Sivarani, T., & Lee, Y. S. 2006, *ApJ*, 652, L37
- Luck, R. E. & Lambert, D. L. 1981, *ApJ*, 245, 1018
- Marsteller, B., Beers, T. C., Rossi, S., Christlieb, N., Bessell, M., & Rhee, J. 2005, *Nucl. Phys A*, 758, 312
- Norris, J. E., Christlieb, N., Korn, A. J., Eriksson, K., Bessell, M. S., Beers, T. C., Wisotzki, L., & Reimers, D. 2007, *ApJ*, 670, 774
- Pandey, G., Lambert, D. L., Rao, N. K., Gustafsson, B., Ryde, N., & Yong, D. 2004, *MNRAS*, 353, 143
- Piskunov, N. E., Kupka, F., Ryabchikova, T. A., Weiss, W. W., & Jeffery, C. S. 1995, *A&AS*, 112, 525
- Plez, B., Brett, J. M., & Nordlund, A. 1992, *A&A*, 256, 551
- Preston, G. W. & Sneden, C. 2001, *AJ*, 122, 1545
- Rossi, S., Beers, T. C., Sneden, C., Sevastyanenko, T., Rhee, J., & Marsteller, B. 2005, *AJ*, 130, 2804

- Ryabchikova, T.A., Piskunov, N.E., Stempels, H.C., Kupka, F., & Weiss, W.W. 1999, *Phys. Scr*, T83, 162
- Ryan, S. G., Aoki, W., Norris, J. E., & Beers, T. C. 2005, *ApJ*, 635, 349
- Sivarani, T., et al. 2006, *A&A*, 459, 125
- Skrutskie, M. F., et al. 2006, *AJ*, 131, 1163
- Snedden, C. 1973, *ApJ*, 184, 839
- Spite, M., et al. 2005, *A&A*, 430, 655
- Stürenburg, S. & Holweger, H. 1990, *A&A*, 237, 125
- Takeda, Y. & Honda, S. 2005, *PASJ*, 57, 65
- Takeda, Y., Zhao, G., Chen, Y.-Q., Qiu, H.-M., & Takada-Hidai, M. 2002, *PASJ*, 54, 275
- Tumlinson, J. 2007, *ApJ*, 665, 1361
- van Dokkum, P. G. 2001, *PASP*, 113, 1420
- Wisotzki, L., Christlieb, N., Bade, N., Beckmann, V., Köhler, T., Vanelle, C., & Reimers, D. 2000, *A&A*, 358, 77
- Woosley, S. E. & Weaver, T. A. 1995, *ApJS*, 101, 181
- Zhang, H. W., Gehren, T., Butler, K., Shi, J. R., & Zhao, G. 2006, *A&A*, 457, 645
- Zhang, H. W. & Zhao, G. 2005, *MNRAS*, 364, 712

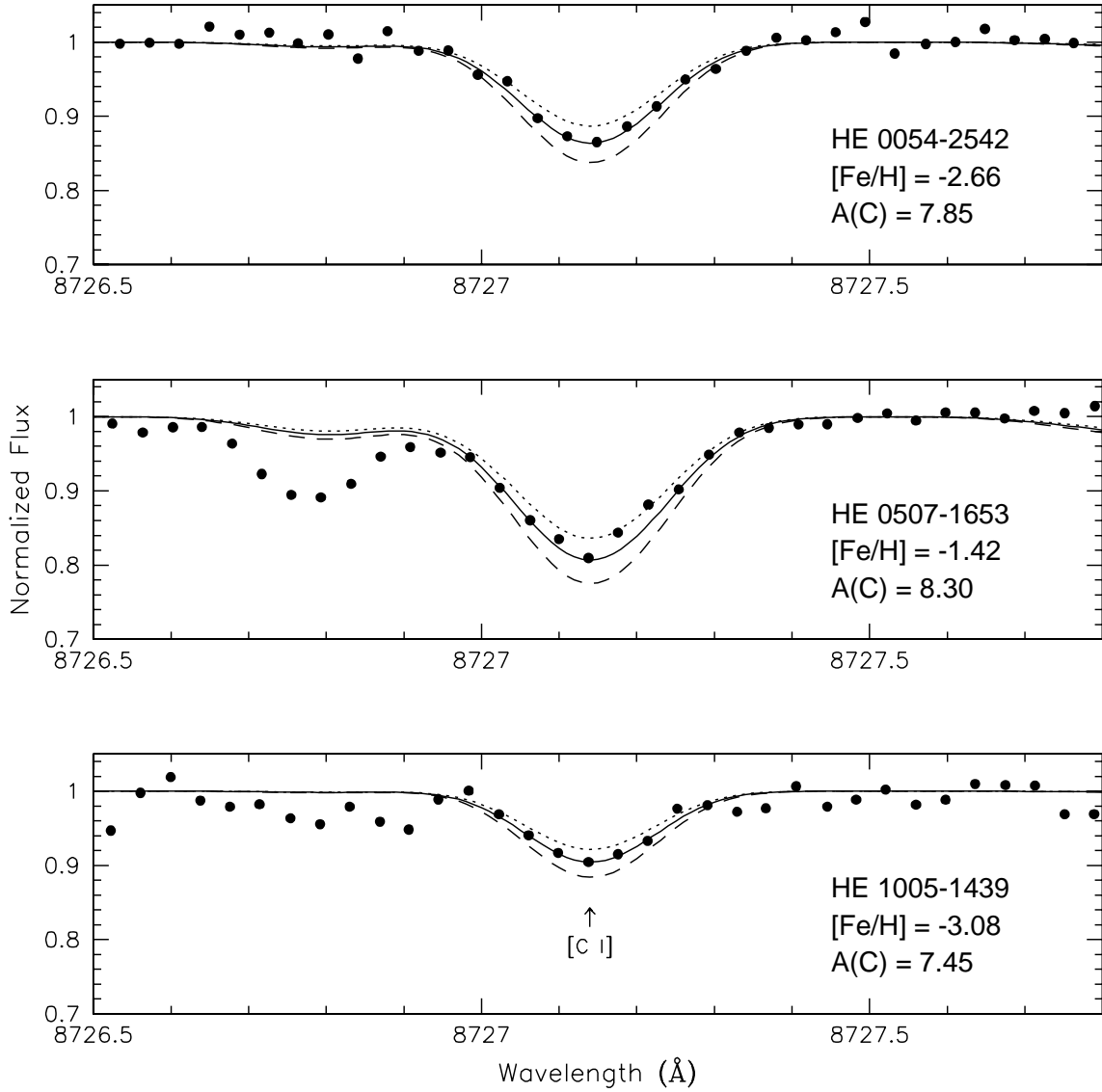


Fig. 1.— High-resolution bHROS spectra (filled circles) and synthetic fits of the 8727 Å region. The solid line is the best-fit synthetic spectrum, characterized by the 1D LTE C abundance given in each panel. The broken lines represent  $\pm 0.10$  dex the best-fit abundance. The [C I] feature at 8727.13 Å is marked by the arrow in the bottom panel.

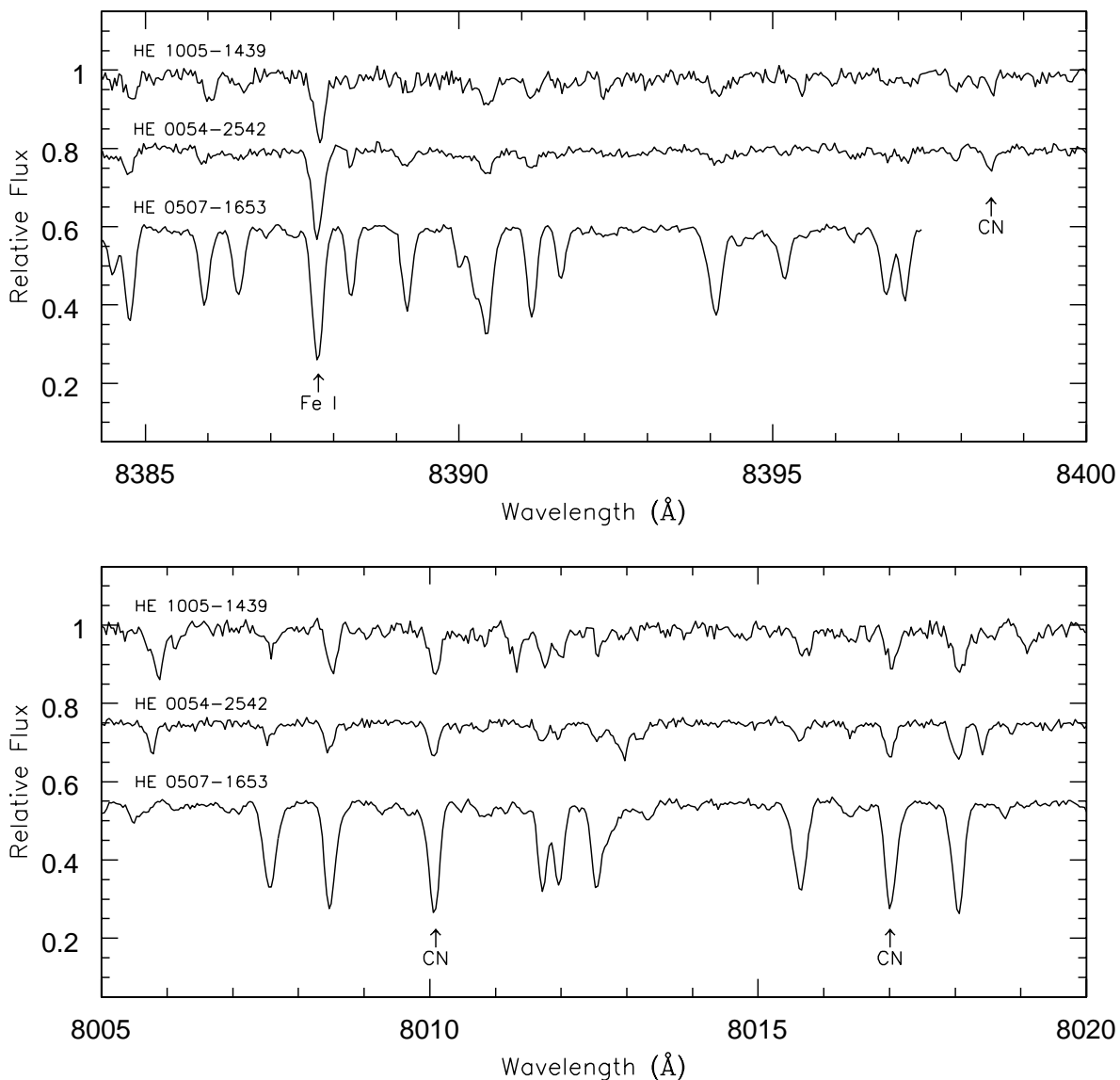


Fig. 2.— High-resolution bHROS spectra of our stellar sample. The lines that have been measured and that have been utilized in the abundance analysis are marked. All of the marked lines have been measured for each star except the CN line at 8398.48 Å, which was measurable only in the spectrum of HE 0054-2542.

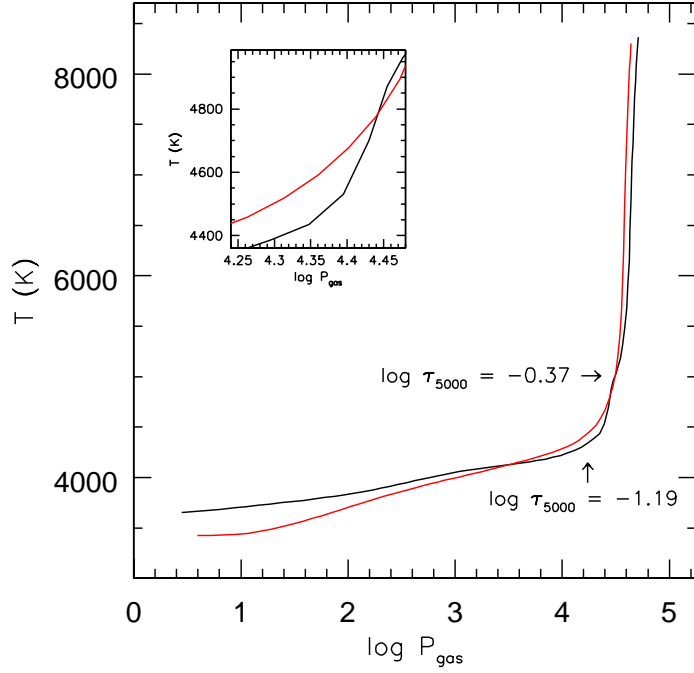


Fig. 3.— Temperature vs. the logarithm of the gas pressure of the 1D LTE C-enhanced ATLAS12 (red) and solar-scaled ATLAS9 (black) models for HE 0054-2542. The inset shows the relations in the line forming region of the spectral features considered in our analysis, as marked by the upper and lower optical depths ( $\log \tau_{5000}$ ) in the main panel.

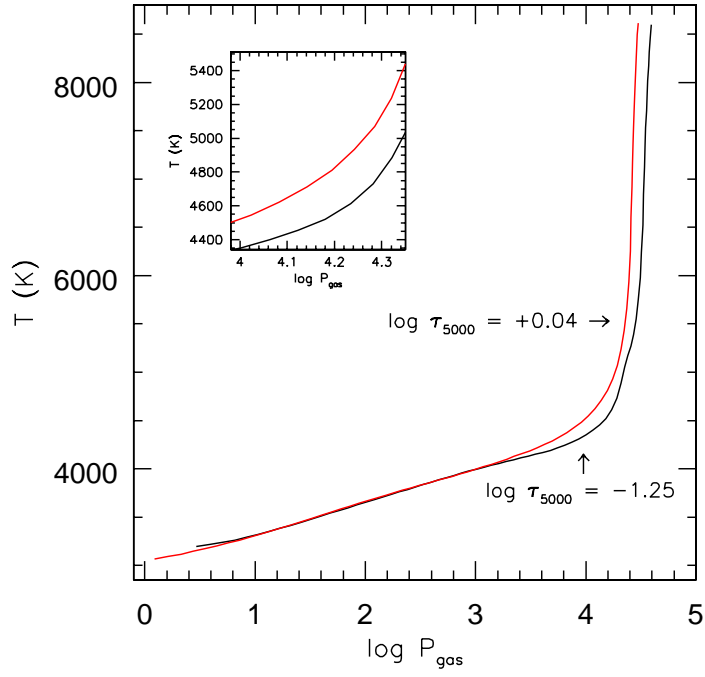


Fig. 4.— The same as Figure 3 but for HE 0507-1653.

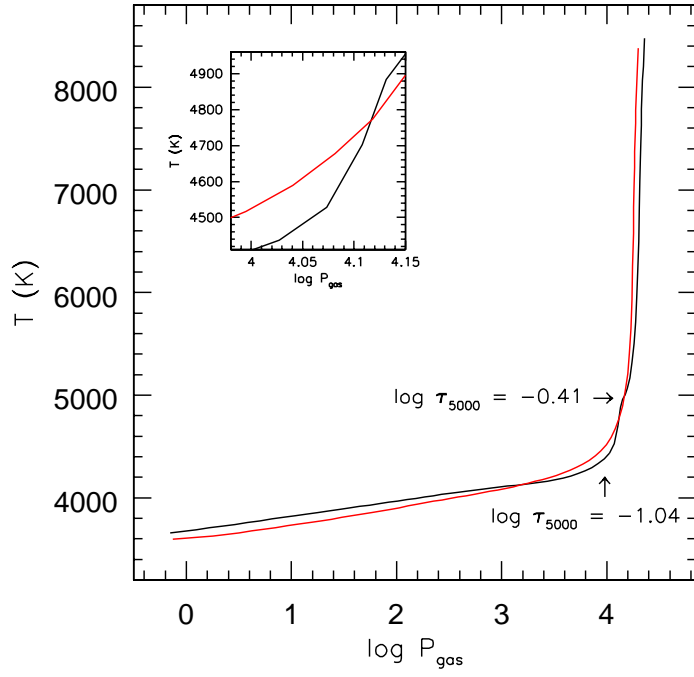


Fig. 5.— The same as Figure 3 but for HE 1005-1439.

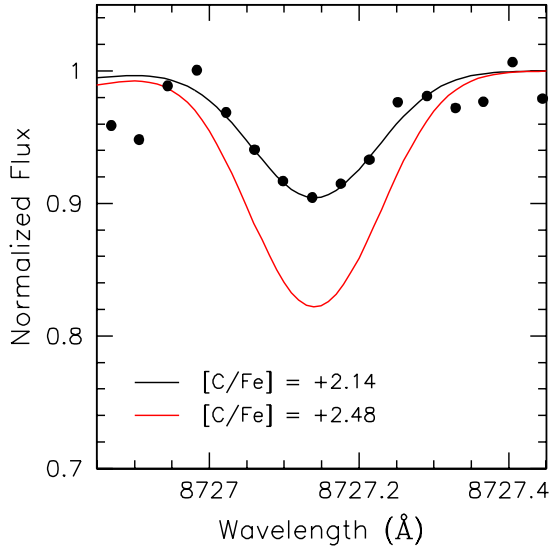


Fig. 6.— Synthetic spectra of the [C I] line of HE 1005-1439. The observed spectrum is given as filled circles, and the best fit synthetic spectrum from our analysis, corresponding to an 1D LTE abundance of  $[C/Fe] = +2.14$ , is shown as the solid black line. The solid red line represents the synthesis of the [C I] feature assuming an abundance of  $[C/Fe] = +2.48$ , the C abundance derived for this star by Aoki et al. (2007). The equivalent width of the synthetic line characterized by the higher abundance is approximately a factor of two larger than that based on our result.

Table 1. Observing Log

Star	UT Date	Exposures	Integration Time (s)
HE 0054-2542	2006 Dec 25	1	3140
	2006 Dec 25	1	3600
	2006 Dec 26	1	3140
HE 0507-1653	2006 Dec 25	2	3140
HE 1005-1439	2006 Dec 25	3	3400
	2006 Dec 25	1	2400
	2006 Dec 26	1	3300

Table 2. Stellar Parameters

Star	Photometry						$T_{\text{eff}}$ (K)	$\log g$ (cgs)	$\xi$ (km s <sup>-1</sup> )	[Fe/H]	[C/Fe]	[N/Fe]	$V_r$ (km s <sup>-1</sup> )	$\sigma_{\text{mean}}$ (km s <sup>-1</sup> )
	$B$	$V$	$R$	$I$	$J$	$K$								
HE 0054-2542	13.57	12.71	...	...	11.19	10.65	5000	2.40	2.00	-2.64	+2.00	+0.80	-230.84	0.44
HE 0507-1653	13.63	12.51	12.00	11.58	10.88	10.32	5000	2.40	2.00	-1.38	+1.30	+0.80	358.94	0.25
HE 1005-1439	14.44	13.52	13.05	12.52	12.24	11.70	5000	1.90	2.00	-3.17	+2.50	+1.80	87.65	0.25

Note. —  $B$  and  $V$  magnitudes for HE 0054-2542 are from Aoki et al. 2002c;  $B, V, R,$  and  $I$  magnitudes for HE 0507-1653 and HE 1005-1439 are from Beers et al. 2007.  $J$  and  $K$  magnitudes for all three stars are from the 2MASS Point Source Catalog (Skrutskie et al. 2006).

Table 3. Equivalent Width Measurements

Species	$\lambda_{\text{rest}}$	$\chi$	$\log gf$	EWs (mÅ)		
	(Å)	(eV)		HE 0054-2542	HE 0507-1653	HE 1005-1439
Fe I...	7181.19	4.22	-0.884	...	24.5	...
	7445.76	4.26	-0.237	9.6	74.5	...
	7723.21	2.28	-3.617	...	19.3	...
	7998.94	4.37	0.048	...	79.9	...
	8046.05	4.42	-0.082	10.1	73.8	...
	8327.06	2.20	-1.525	...	147.3	...
	8387.78	2.18	-1.493	59.4	126.1	38.2
	8688.64	2.18	-1.212	...	...	49.8
	8699.45	4.96	-0.380	...	25.6	...
C I...	7685.20	8.77	-1.519	...	18.3	...
	8335.15	7.69	-0.420	...	...	78.8
	9088.51	7.48	-0.429	130.0	...	115.4
	9094.83	7.49	0.150	185.2	216.8	147.4
CN...	7185.15	0.42	-1.604	9.1	...	12.1
	8010.09	0.19	-1.480	20.9	107.0	24.9
	8017.01	0.22	-1.463	21.7	106.4	25.7
	8053.09	0.26	-1.406	18.7	107.5	22.0
	8054.09	0.28	-1.406	21.5	107.6	18.6
	8064.11	0.29	-1.393	20.7	...	20.3
	8074.43	0.31	-1.380	21.2	...	...
	8345.73	0.65	-1.139	13.8	87.9	23.0
	8398.48	0.73	-1.100	14.0	...	...
K I...	7698.96	0.00	-0.170	35.9	131.8	13.7

Table 4. Derived Abundances and Uncertainties

Species	ATLAS12: C-Enhanced Models			ATLAS9: Solar-Scaled Models		
	HE 0054-2542	HE 0507-1653	HE 1005-1439	HE 0054-2542	HE 0507-1653	HE 1005-1439
[Fe/H] <sup>a</sup>	-2.66	-1.42	-3.08	-2.63	-1.42	-3.09
$\sigma$ . . . . .	0.08	0.15	0.13	0.10	0.16	0.14
$A([\text{C I}])$	7.85	8.30	7.45	7.85	8.26	7.45
$\sigma$ . . . . .	0.12	0.14	0.11	0.11	0.13	0.12
$A(\text{C I})$ .	8.34	8.94	7.90	8.43	9.08	7.99
$\sigma$ . . . . .	0.08	0.34	0.15	0.12	0.42	0.17
$A(\text{N})$ ..	6.36	7.56	6.97	6.21	7.41	6.82
$\sigma$ . . . . .	0.34	0.31	0.33	0.36	0.32	0.37
$A(\text{K})$ ..	3.03	4.40	2.50	3.05	4.45	2.53
$\sigma$ . . . . .	0.08	0.19	0.07	0.09	0.21	0.08

<sup>a</sup>Calculated using the solar Fe abundance of Asplund et al. (2005a)

Table 5. Representative Abundance Sensitiviteis<sup>a</sup>

Species	$\Delta T$ ( $\pm 150$ K)	$\Delta \log g$ ( $\pm 0.50$ dex)	$\Delta \xi$ ( $\pm 0.25$ kms <sup>-1</sup> )	$\Delta[\text{m}/\text{H}]$ ( $\pm 0.50$ dex)	$\Delta A(\text{C})$ ( $\pm 0.50$ dex)	$\Delta A(\text{N})$ ( $\pm 0.50$ dex)	$\sigma_{Total}$ <sup>b</sup>
Fe ....	$\pm 0.11$	0.00	$\pm 0.02$	$\pm 0.04$	$\pm 0.06$	0.00	$\pm 0.08$
[C I] ..	$\pm 0.07$	$\pm 0.18$	0.00	$^{+0.07}_{-0.04}$	$\pm 0.04$	0.00	$\pm 0.12$
C I ...	$\mp 0.08$	$^{+0.07}_{-0.10}$	$\mp 0.05$	0.00	$\mp 0.02$	0.00	$\pm 0.08$
N ....	$\pm 0.38$	$\pm 0.33$	0.00	$^{+0.15}_{-0.10}$	$\pm 0.13$	0.00	$\pm 0.34$
K ....	$\pm 0.11$	0.00	$\pm 0.02$	$\pm 0.04$	$\pm 0.05$	0.00	$\pm 0.08$

<sup>a</sup>Abundance sensitivities are given for HE 0054-2542

<sup>b</sup>The total abundance uncertainty, given by the quadratic sum of the individual parameter sensitivities and the uncertainty in the mean abundance, for abundances based on more than a single spectral line.

Table 6. Carbon and Nitrogen Abundances

Star	$A(\text{C})$	$[\text{C}/\text{Fe}]$	$A(\text{N})$	$[\text{N}/\text{Fe}]$
HE 0054-2542	7.85	+2.12	6.36	+1.24
HE 0507-1653	8.30	+1.33	7.56	+1.20
HE 1005-1439	7.45	+2.14	6.97	+2.27

Table 7. Carbon Abundance Comparison

Star	$[\text{Fe}/\text{H}]$	$A([\text{C I}])$	$A([\text{C I}])$	$A(\text{C I})$	$A(\text{C I})$	$\Delta A(\text{C})^{\text{a}}$	$\Delta A(\text{C})^{\text{a}}$
		1D LTE	3D LTE	1D LTE	1D NLTE	1D LTE	3D + NLTE
HE 0054-2542	-2.66	7.85	7.78	8.34	8.04	+0.49	+0.26
HE 0507-1653	-1.42	8.30	8.33	8.94	8.49	+0.64	+0.16
HE 1005-1439	-3.08	7.45	7.30	7.90	7.60	+0.45	+0.30

$$^{\text{a}}\Delta A(\text{C}) = A(\text{C I}) - A([\text{C I}])$$